Water, salt, and energy balances of the Dead Sea

N. G. Lensky, Y. Dvorkin, and V. Lyakhovsky
Geological Survey of Israel, Jerusalem, Israel

I. Gertman
Israel Oceanographic and Limnological Research, Haifa, Israel

I. Gavrieli
Geological Survey of Israel, Jerusalem, Israel

Received 6 March 2005; revised 13 July 2005; accepted 31 August 2005; published 14 December 2005.

[1] The Dead Sea is a hypersaline terminal lake experiencing a water level drop of about 1 m/yr over the last decade. The existing estimations for the water balance of the lake are widely variable, reflecting the unknown subsurface water inflow, the rate of evaporation, and the rate of salt accumulation at the lake bottom. To estimate these we calculate the energy and mass balances for the Dead Sea utilizing measured meteorological and hydrographical data from 1996 to 2001, taking into account the impact of lowered surface water activity on the evaporation rate. Salt precipitation during this period was about 0.1 m/yr. The average annual inflow is $265-325 \times 10^6$ m^3/yr, corresponding to an evaporation rate of 1.1–1.2 m/yr. Higher inflows, suggested in previous studies, call for increased evaporation rate and are therefore not in line with the energy balance.

Citation: Lensky, N. G., Y. Dvorkin, V. Lyakhovsky, I. Gertman, and I. Gavrieli (2005), Water, salt, and energy balances of the Dead Sea, *Water Resour. Res.*, *41*, W12418, doi:10.1029/2005WR004084.

1. Introduction

[2] Since the first half of the 20th century, the level of the lowest place on Earth, the Dead Sea, has declined by over 20 m [*Gavrieli and Oren*, 2004], and since 1996 the average rate of water level drop is about one m/year. The negative water balance of this unique terminal lake is due to diversion of freshwater from its drainage basin, mainly from water which in the past reached the lake through the lower Jordan River (Figure 1). Yet, despite the environmental impact associated with this decline and the regional and international discussions which aim to resolve and manage the Dead Sea, the water balance of the Dead Sea is not well constrained. The least known parameters in the balances are the evaporation rate and subsurface water inflow. This balance will be crucial for the feasibility study and planning of the proposed "Peace Conduit" project, which aims to convey seawater from the Red Sea to the Dead Sea thereby stabilizing its level [*Gavrieli et al.*, 2005].

[3] Reliable determination of the water balance of hypersaline lakes in general and that of the Dead Sea in particular are more complicated than similar freshwater bodies due to two major factors.

[4] 1. The first is difficulty in determining the amount of evaporated water due to reduced water activity and rate of evaporation: Evaporation from brine surface is less than that from a freshwater surface because the dissolved salts lower the free energy of the water molecules and hence the saturation vapor pressure above the brine. The activity coefficient of water (H_2O) in the brine, β, represents the ratio between vapor pressure above a brine surface and vapor pressure above a freshwater surface at the same temperature [*Stumm and Morgan*, 1981]. The activity of freshwater is $\beta = 1$ by definition, while in hypersaline brines $\beta < 1$ (for the present Dead Sea composition, $\beta \sim 0.67$). Accordingly, the rate of evaporation from such water bodies is not equivalent to that from freshwater under similar conditions [*Salhotra et al.*, 1985, 1987; *Steinhorn*, 1991].

[5] 2. The second factor is difficulty in determining the net water deficit: The decline in the water level of a hypersaline chemically-saturated lake which precipitates salts does not represent the true change in the volume of the lake because the accumulation of the salts effectively raises its floor. The water deficit is therefore larger than it appears from simple level changes. In the Dead Sea, halite (NaCl) began to precipitate in 1979 [*Steinhorn*, 1983], and since then, continues to precipitate. The rate of accumulation has been estimated to be several centimeters per year, from chemical considerations [*Gavrieli*, 1997].

[6] To resolve the long-term evaporation rate and water balance of the Dead Sea, we adopt the energy budget method, which is considered the preferential technique for long-term monitoring [*Winter et al.*, 2003]. A somewhat similar but simplified approach was applied to the Dead Sea by *Stanhill* [1994] and *Neumann* [1958] utilizing a limited data set. We first present a formulation for the simultaneous determination of the energy, water and salt balances for hypersaline lakes. This approach requires reliable meteorological and limnological data. Using detailed data that accumulated from a buoy in the center of the Dead Sea since 1992, we evaluate annual inflow, rate of evaporation

0043-1397/05/2005WR004084

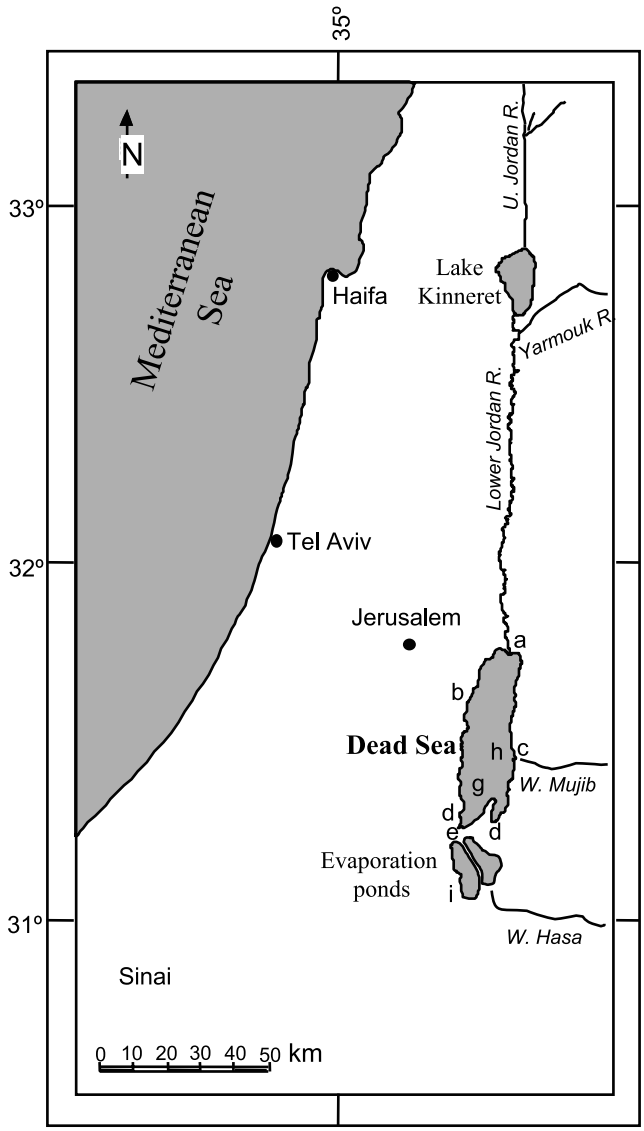

Figure 1. Location map. Major freshwater inflow: Jordan River (a), En Fesh'ha springs (b), and Arnon-Mujib (c). Dead Sea brine is pumped from location d to the evaporation ponds and the rejected concentrated end brine is diverted back into the Dead Sea at location e. The locations of the meteorological and hydrographic stations are EG100 (g) and EG320 (h). Sedom (i) is located within the evaporation ponds.

and rate of salt precipitation. Figure 2 presents a flowchart for the methodological approach with reference to sections in this article, main equations, figures, and tables.

2. Hydrographical Setting of the Dead Sea

[7] The Dead Sea is a terminal hypersaline lake (salinity ~277 g/kg) with extremely high density (~1240 kg/m^3 at 23°C). The present (2005) volume of the Dead Sea is ~132 km^3, with surface area of ~625 km^2, maximum depth of ~300 m and surface level at ~418 meters below mean sea level. It forms the lowest place on Earth, which currently is declining by ~1 m/yr. At the time of the first in-depth study of the properties of the Dead Seawater column, in 1959–1960, the lake was stratified (meromictic) with the shallow southern basin flooded (today it is the site of industrial evaporation ponds, Figure 1). Somewhat less saline upper water mass (epilimnion) floated over a denser lower water mass (hypolimnion) [*Neev and Emery*, 1967]. The lower water mass had been isolated for at least several centuries [*Steinhorn et al.*, 1979; *Stiller and Chung*, 1984], was anoxic and contained H_2S. It should also be noted that in the past 40 years, the solar radiation in the Dead Sea Rift Valley in general, and in the Dead Sea in particular, has declined by more than 10% [*Stanhill and Cohen*, 2001].

[8] In 1976, following the negative water budget and lake level drop, the very shallow southern Dead Sea dried out. With the increase in salinity of the epilimnion, its density increased and the stability of the upper layer that had existed during the meromictic state weakened. This finally led to a complete overturn and homogenization and oxidation of the entire water column in 1979 [*Beyth*, 1980; *Steinhorn et al.*, 1979; *Steinhorn and Gat*, 1983]. Since then, the Dead Sea experiences mostly annual stratification and overturns (holomictic regime), while its salinity and temperature continuously rise at overturn and its water level declines [*Anati and Stiller*, 1991; *Gertman and Hecht*, 2002]. This trend was discontinued twice, following large freshwater inflow during the particularly rainy winters of 1979/1980 and 1991/1992. These inflows lead to the dilution of the surface water and to the development of a stabilizing halocline that maintained the stratification for 3–4 years [*Anati and Stiller*, 1991; *Beyth et al.*, 1993]. During holomictic years, stratification develops in spring due to the warming of the upper water layer, or less commonly in late winter due to limited dilution of the water as a result of winter rain floods. During summer months, increased evaporation results in a salinity rise of the epilimnion and the development of a destabilizing halocline. However, stratification is maintained by the stabilizing thermocline (generally located between 25 and 30 m depth). Surface water temperatures reach up to 35°–36°C, while the

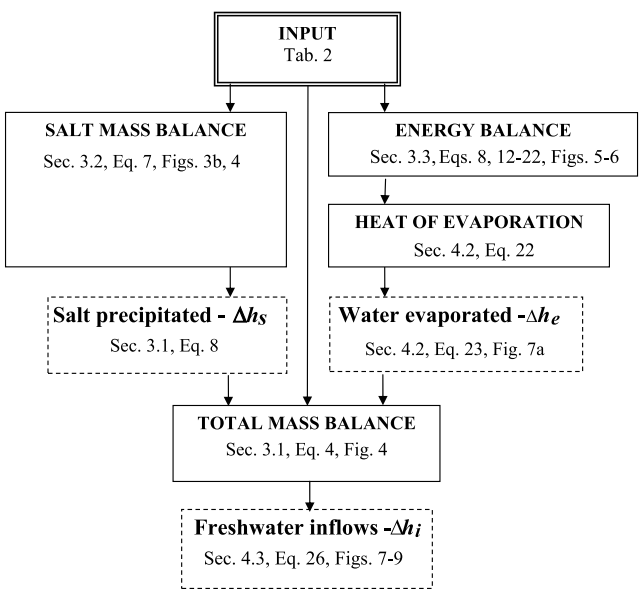

Figure 2. Flowchart for the solution of the mass and energy balances. The dashed frames are the three unknowns, which are solved by a set of the three balance equations.

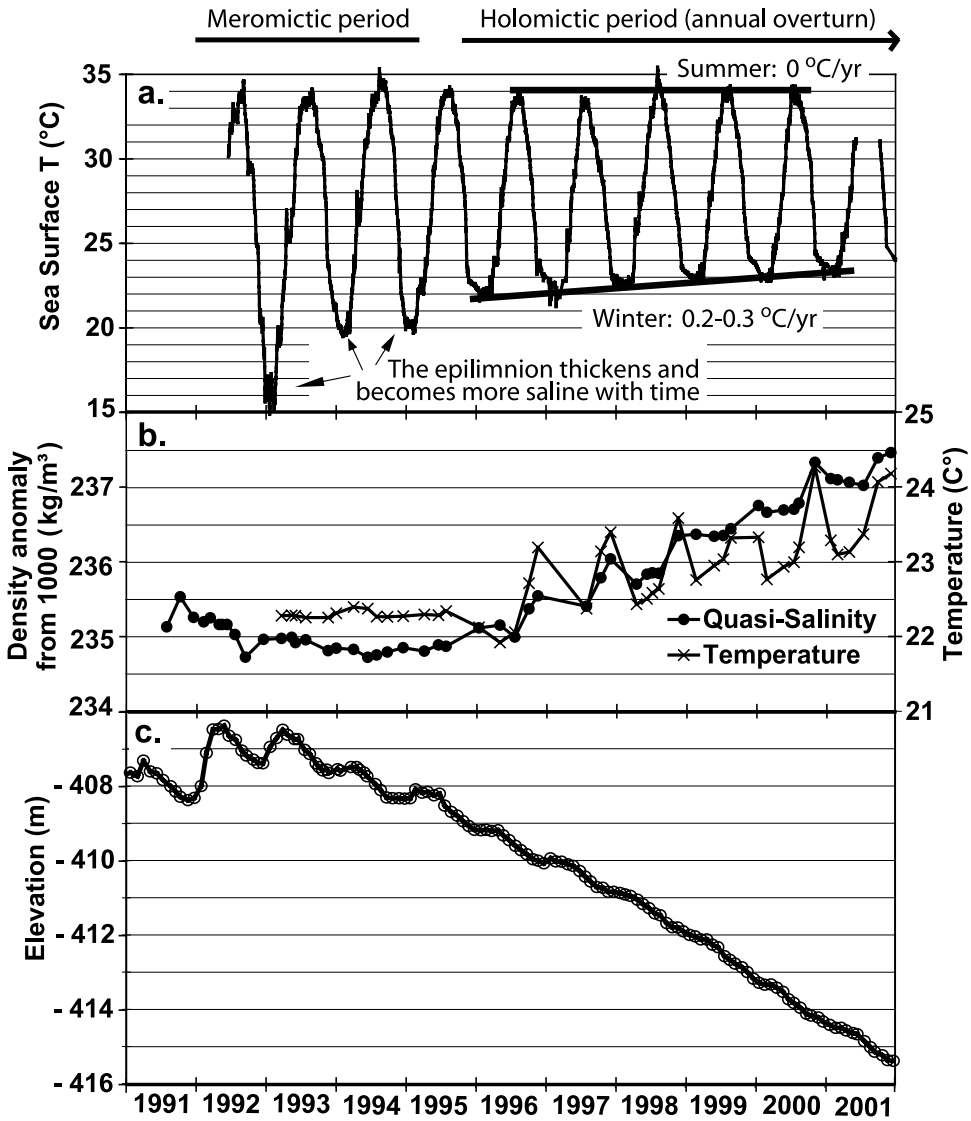

Figure 3. (a) Surface temperature measured in the Dead Sea at station EG100 (see Figure 1 for location). In 1992 a meromictic period began, following a very rainy winter with unusually high inflow from the Jordan River and other sources. This period ended at the end of 1995 when the lake overturned and began a holomictic period. In the holomictic period the Dead Sea water column overturned every winter, and thus the winter surface temperature represents the whole water column. The interannual temperature rise is 0.2–0.3°C, after *Hecht and Gertman* [2003]. The low surface temperature during winters of the meromictic period is due to intensive cooling of the epilimnion, while in the holomictic period the whole water body is cooled (about 10 times larger in volume) and thus winter temperature are higher. (b) Averaged quasi-salinity (σ_{25}) (see text for definition) and temperature of the Dead Sea deep water body (below 100 m). (c) Dead Sea level. Note the surface elevation during the rainy years 1992–1993 and the continuous decrease of the Dead Sea level from 1996 to 2001 at a rate of ~1 m/yr.

temperature of the water mass below the thermocline remains stable in the range of 22–23°C. Overturn occurs following the autumn cooling of the upper water column and the consequent increase in its density. Figure 3a shows the surface water temperature interannual fluctuation during 1992–2001. The surface temperature in winters, when the lake is homogeneous, represents the temperature of the entire water column. During the holomictic years (1996–2001), this temperature increased from winter to winter by 0.2–0.3°C/yr [*Hecht and Gertman*, 2003]. This trend is compatible with the increase in the temperature of the deep water (deeper than 100 m, Figure 3b). Figure 3b also presents the change in the salinity of the deep water, given in quasi-salinity units (σ_{25}). The latter was defined by *Anati* [1997] as the deviation of the brine density at 25°C from density of freshwater. During the same holomictic period, the quasi-salinity of the deep water increased annually by about 0.3 kg/m^3/yr [*Gertman and Hecht*, 2002], corresponding to a salinity increase of 0.24 g/kg/yr. The annual heating and increase in salinity are related to the negative water balance of the lake, as manifested by the annual water level drop during this period (Figure 3c).

[9] Natural water inflows to the Dead Sea during the first half of the 20th century were estimated to be in the range of

Table 1. Estimated Annual Inflow Volumes to the Dead Sea During the Drought Years of 1996–2001

Source	Volume, $\times 10^6$ m^3/yr	References
Jordan River	60–150	*Dalin* [1988], *Holtzman et al.* [2005]
Eastern side of the Dead Sea (mainly through Mujib, Hasa, Zerka Ma'in and El Karek Wadis)	70–150	*Salameh and Udluft* [1985]
Western side of the Dead Sea (mainly En Fesh'ha, Kane, and Samar springs)	80–120	Israel Hydrological Service
Direct precipitation (70 mm/yr)	45	based on average rainfall of 70 mm/yr
Estimated flood water	10	
Sum	265–475	

1600–2000 $\times$ 10^6 m^3 per year [*Klein*, 1998; *Neumann*, 1958; *Salameh and El-Naser*, 1999]. The volume of water reaching the Dead Sea today is substantially lower, with estimates varying between <475 $\times$ 10^6 m^3/yr (Table 1) and >1000 $\times$ 10^6 m^3/yr [*Salameh and El-Naser*, 1999]. The difference (>500 $\times$ 10^6 m^3/yr) is due to different estimations of the unobserved subsurface inflow. The higher inflow estimation is based on a higher estimation of evaporation rate (2 m/yr, from pan evaporation) [*Salameh and El-Naser*, 1999]. A much lower evaporation rate, 1.05 m/yr, was estimated for the Dead Sea based on an energy balance for the period of 1980s and 1990s [*Stanhill*, 1994]. Available standard pan evaporation measurements from Sedom in the southern Dead Sea basin (Figure 1), are difficult to use to resolve the evaporation rate from the Dead Sea for three reasons. (1) The lowered water activity in the Dead Sea brine [*Salhotra et al.*, 1985]. (2) Reduced evaporation in an open lake compared to pan [*Morton*, 1983]. (3) According to *Alpert et al.* [1997], the local conditions at Sedom are different than those in the northern basin, leading to enhanced evaporation. To resolve the evaporation from Dead Sea, we apply the energy balance method on a hydrometeorological data set measured in a buoy located in the middle of the Dead Sea (Figure 1).

[10] A water balance of the Dead Sea must also take into account the industrial activities in the Dead Sea chemical industries (DSCI, both Israeli and Jordanian). These pump brine from the Dead Sea into evaporation ponds which are located in the otherwise dry southern Dead Sea basin. Here salts precipitate and are harvested by the industry. The concentrated end brine is then returned to the lake with a net water loss of about 250 $\times$ 10^6 m^3/yr [*Gavrieli and Oren*, 2004].

[11] Below we present a formulation for the mass and heat balances for salt lakes (section 3). We then apply this formulation to solve for the inflow, rate of evaporation and the rate of salt precipitation in the Dead Sea, based on recently measured meteorological and hydrographical data (section 4).

3. Formulation of the Mass and Heat Balances

3.1. Total Mass Balance

[12] Let us consider a saline lake with bulk density ρ and total volume V_t (see Figure 4a and notation section). The total mass of the brine, m_t, is equal to the sum of mass of dissolved salts, m_s, and the mass of fresh water, m_w:

$$m_t = m_s + m_w = \rho V_t. \quad (1)$$

[13] With time, several processes change the mass balance (Figure 4b). Evaporation reduces the mass of water in the brine by Δm_e, whereas water enters the lake in the form of rivers, runoff, observed springs, and rain and subsea inflow, the total being Δm_i. Salt precipitation reduces the mass of dissolved salts by Δm_s. In the case of the Dead Sea, additional uncommon factors need to be included in the balances: the DSCI pump Δm_p of the Dead Sea brine into evaporation ponds, and reject Δm_r of the evaporated end brine back to the lake. The change of the mass of the brine after a period Δt, is

$$\Delta m_t = \Delta m_e + \Delta m_s - \Delta m_i + \Delta m_p - \Delta m_r. \quad (2)$$

As a result of the above processes, the new mass of the brine after a period Δt is

$$m_t - \Delta m_t = (\rho + \Delta\rho)(V_t - \Delta V_l - \Delta V_s), \quad (3)$$

where $\Delta\rho$ is the change in density of the brine, ΔV_s is the volume of salt precipitated on the sea bottom, and ΔV_l is the volume loss as appears from water level drop. Substituting (1) and (2) into (3), and neglecting the second-order terms $\Delta\rho\Delta V_l$ and $\Delta\rho\Delta V_s$ ($\Delta\rho \ll \rho$, $\Delta V_s \ll V_t$ and $\Delta V_l \ll V_t$), yields

$$\Delta m_e + \Delta m_s - \Delta m_i + \Delta m_p - \Delta m_r = \rho\Delta V_l + \rho\Delta V_s - \Delta\rho V_t. \quad (4)$$

[14] The equation of mass balance contains three unknowns: mass of water evaporated, Δm_e, mass of total water inflow, Δm_i, and mass of salt precipitated, Δm_s. The total inflow is solved after the rate of precipitation is solved

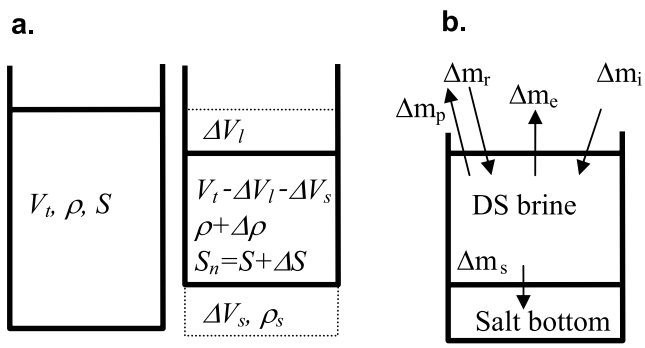

Figure 4. (a) Sketch of volume changes due to evaporation and precipitation. (b) Mass balance.

from salt balance considerations and the evaporation rate from energy balance considerations (sections 3.2 and 3.3, respectively).

3.2. Salt Mass Balance

[15] The salinity of the brine is the ratio between the mass of dissolved salts and the total mass of the brine:

$$S = \frac{m_s}{m_t}. \tag{5}$$

After a given time (Δt), the new salinity ($S_n = S + \Delta S$) is the ratio between the new mass of dissolved salts and the new total mass of the brine ($m_t - \Delta m_t$). The new mass of dissolved salts is the sum of masses of dissolved salts pumped from the Dead Sea ($\Delta m_p S$), end brines that return from the DSCI, ($\Delta m_r S_r$), salts added by the inflow ($\Delta m_i S_i$) and the mass of salt precipitated from the brine (Δm_s):

$$S_n = \frac{m_s - \Delta m_s - \Delta m_p S + \Delta m_r S_r + \Delta m_i S_i}{m_t - \Delta m_t}. \tag{6}$$

[16] After substitution of (3) in the denominator, substitution of $m_s = S \cdot m_t$ (5) in the numerator, using the relation $\Delta V_s = \Delta m_s/\rho_s$ (volume of salt precipitated is the mass divided by density of the salt) and neglecting the second-order term $\Delta\rho\Delta V_l$, we get

$$\Delta m_s = \frac{(\rho\Delta V_l - \Delta\rho V_t)S_n - m_t\Delta S - \Delta m_p S + \Delta m_r S_r + \Delta m_i S_i}{1 - S_n\rho/\rho_s}. \tag{7}$$

[17] This equation can now be substituted into the total mass balance (4). The remaining unknown is then the amount of water evaporated, Δm_e, which is solved from energy balance considerations in section 3.3.

3.3. Energy (Heat) Balance

[18] The energy budget for water bodies is generally expressed as [*Anderson*, 1952]

$$Q_n = Q_{SN} - Q_{LW} - Q_e - Q_c + Q_{AD}. \tag{8}$$

[19] The energy flux terms (W/m^2), shown in Figure 5, are Q_{SN}, net solar radiation incident into the water body; Q_{LW}, net energy lost through the exchange of long-wave radiation between the atmosphere and the body of water; Q_e, evaporative heat flux; Q_c, energy conducted to the atmosphere as sensible heat flux; Q_{AD}, net advected heat into the water body; Q_n, net heat flux, which is the change in energy stored in the body of water. Below we present the different energy flux components in terms of measurable parameters.

3.3.1. Net Heat Flux Q_n and the Net Advected Heat Flux Q_{AD}

[20] The net heat flux Q_n, or the change in energy stored in the water body, is manifested by the change in the lake's temperature and mass after the considered period. The net annual energy change for a homogeneous water body, E_n, is related to the mass of the brine, m_t, its surface temperature, T_s, temperature change, ΔT, and the change in the total mass of the brine, Δm_t:

$$E_n = c_p[T_s m_t - (T_s + \Delta T)(m_t - \Delta m_t)], \tag{9}$$

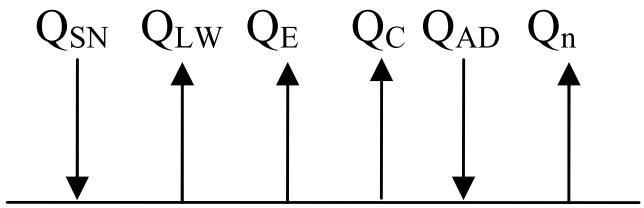

Figure 5. Energy balance. Q_{SN}, net solar radiation; Q_{LW}, net long-wave radiation; Q_E and Q_C, evaporation and conductive heat flux; Q_{AD}, advected heat flux Q_n, net heat flux.

where c_p is the specific heat capacity of the brine. The net energy is translated to heat flux, averaged for the Δt period over the area, A, of the lake:

$$Q_n = \frac{E_n}{A\Delta t} = c_p\frac{\Delta m_t T_s - m_t\Delta T + \Delta m_t\Delta T}{A\Delta t}. \tag{10}$$

[21] The second-order term, $\Delta T \cdot \Delta m_t$, is negligible for $\Delta T \ll T$ and $\Delta m_t \ll m_t$. The first term is related to the change in mass, or the net advected heat flux, and the second term to other processes that change the temperature of the water body.

[22] The advected heat flux, Q_{AD}, is the net energy gained or lost by a body of water through the ingress or egress of water. Advected masses may result from surface inflow, evaporation and the other terms of equation (2).

$$Q_{AD} = c_p\frac{\Delta m_i T_i + \Delta m_r T_r - \Delta m_p T_s - \Delta m_e T_s - \Delta m_s T_s}{A\Delta t}. \tag{11a}$$

[23] Using the definition of Δm_t (2) and adding and subtracting T_s from every component in (11a), the advective heat flux is represented in the following form:

$$Q_{AD} = c_p\frac{\Delta m_i(T_i - T_s) + \Delta m_r(T_r - T_s) + \Delta m_t T_s + \Delta m_t\Delta T}{A\Delta t}. \tag{11b}$$

[24] Since we are interested in the calculation of the evaporative heat flux, we have to calculate the difference between the net heat flux (10) and the net advective heat flux (11b) rather than calculate them separately. Subtracting Q_{AD} from Q_n yields

$$Q_n - Q_{AD} = -c_p\frac{m_t\Delta T + \Delta m_i(T_i - T_s) + \Delta m_r(T_r - T_s) + \Delta m_t\Delta T}{A\Delta t}. \tag{12}$$

3.3.2. Net Solar Radiation Q_{SN}

[25] The net solar short-wave radiation penetrating into the water, Q_{SN}, is calculated from the solar radiation measured above the lake surface, Q_S:

$$Q_{SN} = \alpha \cdot Q_S, \tag{13}$$

where α is the fraction of radiation that penetrates into the water surface [*Payne*, 1972; *Ryan and Harleman*, 1973].

3.3.3. Net Long-Wave Radiation Q_{LW}

[26] The net long-wave radiation is the difference between the upward infrared radiation emitted by the water

body and the atmospheric radiation reaching the surface of the water body. Several bulk formulas for the net long-wave radiation at the sea surface exist [*Bignami et al.*, 1995]:

Brunt [1932]

$$Q_{LW} = k_b\varepsilon \cdot T_s^4(0.39 - 0.05\sqrt{e_a})(1 - 0.8C)$$

Berliand and Berliand [1952]

$$Q_{LW} = k_b\varepsilon \cdot T_a^4(0.39 - 0.05\sqrt{e_a})(1 - 0.8C) + 4k_b\varepsilon \cdot T_a^3(T_s - T_a)$$

Clark et al. [1974]

$$Q_{LW} = k_b\varepsilon \cdot T_s^4(0.39 - 0.05\sqrt{e_a})\left(1 - 0.69C^2\right) + 4k_b\varepsilon \cdot T_s^3(T_s - T_a)$$

Efimova [1961]

$$Q_{LW} = k_b\varepsilon \cdot T_a^4(0.254 - 0.0495e_a)(1 - 0.8C)$$

Bunker [1976]

$$Q_{LW} = 0.22k_b\varepsilon \cdot T_s^4(11.7 - 0.23e_a)(1 - 0.68C) + 4k_b\varepsilon \cdot T_a^3(T_s - T_a)$$

Anderson [1952]

$$Q_{LW} = k_b\varepsilon\left(T_s^4 - T_a^4(0.74 + 0.0049e_a)\right)(1 - 0.8C)$$

Swinbank [1963]

$$Q_{LW} = k_b\varepsilon\left(T_s^4 - 9.36 \cdot 10^{-6}T_a^6\right)(1 - 0.8C)$$

Bignami et al. [1995]

$$Q_{LW} = k_b\varepsilon T_s^4 - k_b T_a^4(0.653 + 0.00535e_a)\left(1 + 0.1762 \cdot C^2\right)$$

U.S. Environmental Protection Agency (*USEPA*) [1984]

$$Q_{LW} = k_b\varepsilon T_s^4 - k_b T_a^4(0.5097 + 0.06575\sqrt{e_a})\left(1 + 0.17C^2\right). \quad (14)$$

[27] In these equations, T_s and T_a are the sea surface and air temperature in °K, k_b is the Boltzmann coefficient, ε is the emissivity of the water body and C is cloud cover. The atmospheric vapor pressure, e_a, is calculated from the measured relative humidity (RH) and the saturation vapor pressure (e_{sat}) at ambient air temperature:

$$e_a = RH \cdot e_{sat}(T_a), \quad (15)$$

where we use the Magnus-Tetens formula for the saturation vapor pressure:

$$e_{sat}(T) = 6.105 \cdot \exp\left(\frac{17.27 \cdot T}{T + 237.7}\right), \quad (16)$$

where T is temperature in °C and e_{sat} in mbar [*Barenbrug*, 1974].

3.3.4. Evaporative Heat Flux Q_e

[28] The heat flux of evaporation is proportional to the difference between saturation vapor pressure above the saline lake, e_{brine}, and the atmospheric vapor pressure, e_a (15):

$$Q_e = f(w)(e_{brine} - e_a). \quad (17)$$

The vapor pressure of a brine, e_{brine}, is lower than that of freshwater, e_{sat}, by a factor β, which is the water activity [*Salhotra et al.*, 1985]:

$$e_{brine} = \beta \cdot e_{sat}(T_s). \quad (18)$$

The wind function, $f(w)$, accounts for the effect of air convection above the water surface on the rate of evaporation. This is the least known parameter in the energy balance, thus the Bowen's approach [*Anderson*, 1952; *Bowen*, 1926] is widely used to eliminate the wind function out of consideration, as described below.

3.3.5. Conductive (Sensible) Heat Flux Q_C

[29] Conductive heat flux, Q_c, is driven by the temperature difference between the water surface and the atmosphere; it can be either a source or a sink of heat for the water body, depending on the difference between the temperatures:

$$Q_c = c_b \frac{P}{1000} f(w)(T_s - T_a), \quad (19)$$

where P is the atmospheric pressure (mbar) and c_b is the Bowen's constant, typically 0.61 mbar/°C [*Anderson*, 1952; *Bowen*, 1926; *Rubin and Atkinson*, 2001]. Equation (19) includes the same wind function, $f(w)$, as in (17). The use of the same wind function in (19) as in (17), is based on the similarity between heat and vapor transport [*Bowen*, 1926; *Businger*, 1973]. This approach allows eliminating the wind function by combining (17) and (19):

$$Q_c = Q_e \cdot B, \quad (20)$$

where B is the Bowen ratio:

$$B = c_b \frac{T_s - T_a}{e_{brine} - e_a} \frac{P}{1000}, \quad (21)$$

and P is the atmospheric pressure. The conductive heat, Q_c, is now expressed in terms of the evaporative heat, Q_e. Substituting (20) into (8) enables expressing evaporation heat flux in terms of heat flux components:

$$Q_e = \frac{Q_{SN} - Q_{LW} - Q_n + Q_{AD}}{1 + B}. \quad (22)$$

This equation enables calculating the evaporative heat flux based on measurable meteorological and hydrological quantities without the need of the wind function.

3.3.6. Evaporation Rate Δh_e

[30] The evaporative heat flux (22) is related to the rate of evaporation, Δh_e (m/yr) through the latent heat of vaporization, L_e:

$$\Delta h_e = \Delta t \frac{Q_e}{\rho L_e} = \frac{\Delta t}{\rho L_e} \frac{Q_{SN} - Q_{LW} - Q_n + Q_{AD}}{1 + B}. \quad (23)$$

Note that the density and the latent heat of vaporization refer to the brine. The mass of evaporated water is $\Delta m_e = \Delta h_e \rho_w A$.

[31] We now have a set of three equations (4, 7, 23) with three unknowns (Δm_i, Δm_s, Δm_e) expressed through measurable data and physical properties of the brine and the atmosphere above it.

4. Application of the Model to the Dead Sea

[32] The solution of the mass and energy balances for the Dead Sea is based on the data set collected by *Gertman and Hecht* [2002] at the hydrometeorological buoy which was anchored in the Dead Sea (station EG100, see Figure 1 for location) and operated from 1992 to 2001. The data set consists of meteorological and hydrographical measurements and includes air temperature (T_a), relative humidity (RH), incoming solar radiation (Q_S), atmospheric pressure (P), surface water temperature (T_s) and temperature profile down to 40 m below the sea surface. The data is averaged and recorded every 20 min. The balances are calculated for all data records (every 20 min) and then averaged over each year during the holomictic period 1996–2001. The Dead Sea level is measured on a monthly basis by the Israel Hydrological Service. Hydrographical profiles taken in intervals of two months at the deepest part of the Dead Sea, at site EG320 (water depth ~310 m, Figure 1), provide the vertical distribution of temperature, salinity and density and the annual change in surface temperature (ΔT), salinity (ΔS) and density ($\Delta\rho$) of the bulk Dead Sea (Figure 3b).

[33] During the winters of 1996–2001, the Dead Sea water body was well mixed with homogeneous distribution of water temperature and composition. Therefore the measurements taken at the sampling station (EG-320) in consecutive winters represent the annual variations of the heat stored in the Dead Sea, the salinity of the brine and the total mass of the Dead Sea brine. Yearly balances are calculated based on the meteorological data for the holomictic period 1996–2001. The current situation of very low water inflow into the Dead Sea allows significant simplification of the balances. On an annual basis, the total inflow is less than 1% of the volume of the lake. The low inflow has negligible impact on the salt and heat balances, but is an important component in the water mass balance. The adjacent freshwater Lake Kinneret (Figure 1), which receives relatively large volume inflow, including saline springs, require a more complex solution of the balances as presented by *Assouline* [1993].

[34] Below we calculate the balances of the Dead Sea and determine the water inflow, rate of evaporation and mass of precipitated salt for year 1999 (Table 2). The heat and mass balances for this year is the closest to the average annual balances calculated for each year during the holomictic period. The interannual variations of the balances during the holomictic years are discussed in section 4.4.

4.1. Salt Accumulation at the Bottom of the Dead Sea

[35] The observed annual rise in the salinity of the Dead Sea brine ($\Delta S = 0.24$ g/kg per year, Figure 3b) is lower than that expected from the negative water balance. This is attributed to the precipitation of salt (halite) from the saturated brine [*Gavrieli*, 1997]. Using the equation of salt balance (7) and the measured parameters, we solve for the mass of precipitated salts, Δm_s. It is useful to express Δm_s in units of volume per unit area. The surface area of the lake, A, is assumed to be constant during a year ($\Delta A \ll A$). This enables expressing the masses involved in the mass and salt balances in terms of volume per unit area and density:

$$\begin{aligned}
\Delta m_i &= \rho_i \Delta V_i = \rho_i \Delta h_i A \\
\Delta m_e &= \rho_w \Delta V_e = \rho_w \Delta h_e A \\
\Delta m_s &= \rho_s \Delta V_s = \rho_s \Delta h_s A \\
\Delta m_p &= \rho \Delta V_p = \rho \Delta h_p A \\
\Delta m_r &= \rho_r \Delta V_r = \rho_r \Delta h_r A \\
V_t &= h_t A \\
\Delta V_l &= \Delta h_l A \\
\Delta V_s &= \Delta h_s A.
\end{aligned} \tag{24}$$

[36] Substitution of (24) into the salt balance (7) yields

$$\Delta h_s = \frac{(\Delta h_l \rho - h_t \Delta\rho) S_n - h_t \rho \Delta S - \Delta h_p \rho S + \Delta h_r \rho_r S_r + \Delta h_i \rho_i S_i}{\rho_s - (\rho + \Delta\rho) S_n}. \tag{25}$$

[37] The contribution of inflow to the salt balance is very low due to their relatively low volume and salinity ($S_i <$ 10 g/kg on average) and therefore the term $\Delta h_i \rho_i S_i$ can be neglected. One can argue that the salinity is higher in the unobserved inflow. However, as will be shown below, the volume of unobserved inflow is no more than a few tens of 10^6 m^3/yr. Substituting the measured data from Table 2 into the salt balance (25), the calculated rate of salt accumulation at the bottom of the Dead Sea is $\Delta h_s = 0.10$ m/yr. Even if we assume Dead Sea salinity for the unobserved inflow, which is probably a wild overestimate, the contribution to the calculated salt layer is <0.02 m/yr. This would have a minor effect on the rest of the balances. The calculated salt precipitation is in the range of previous estimates based on changes in the composition of the brine [*Gavrieli*, 1997], measurements of samples collected from the bottom [*Levy*, 1992] and from sediment traps [*Stiller et al.*, 1997].

4.2. Evaporation

[38] The evaporation rate from the Dead Sea surface is calculated from the energy balance (23). Figure 6 presents the calculated energy balance terms and shows that the largest component in the balance is the forcing solar radiation (Q_{SN}). The net long-wave radiation (Q_{LW}) is determined independently from equations (14). Table 2 presents these calculated Q_{LW} values for the Dead Sea in 1999, which span over the range of 68–108 W/m^2. The minimum and maximum values of the evaporative flux (Q_e) depend on the maximum and minimum Q_{LW} values, respectively (22), as shown in Figure 6. An additional, but relatively minor source of uncertainty in the calculated

Table 2. Input Data, Physical Properties, and Some Results of the Balances of the Dead Sea, 1999[a]

	Description	Value	Units
Hydrographic data			
V_t	volume of the Dead Sea	132	10^9 m^3
A	area of the Dead Sea	625	10^6 m^2
Δh_l (1)	water level drop	1.04	m/yr
ΔV_p (2)	volume pumped	500	10^6 m^3/yr
ΔV_r (2)	volume of rejected end brines	250	10^6 m^3/yr
ΔV_i (3)	freshwater inflow - observed	265–475	10^6 m^3/yr
ΔT (4)	temperature rise	0.2–0.3	°C/yr
ΔS (4)	salinity increase	0.00024	kg/kg/yr
S_r (2)	salinity of rejected end brines	0.350	kg/kg
ρ (4)	density of the Dead Sea (at 23°)	1240	kg/m^3
$\Delta\rho$ (4)	annual increase of density	0.22	kg/m^3
ρ_w	freshwater density	1000	kg/m^3
ρ_s	halite (solid) density	2200	kg/m^3
ρ_r (2)	rejected end brines density	1350	kg/m^3
Physical properties			
ε (5)	emissivity	0.97 ± 0.1	
α (7)	1 − albedo	0.940	
K_b	Boltzmann coefficient	5.67×10^{-8}	W/m^2 K^4
$L_{e,DS}$ (6)	latent heat of Dead Sea brine	2.49	10^6J/kg
Cp_{DS} (6)	heat capacity of Dead Sea brine	3030	J/kg/C
Result, highest estimates for 1999			
Δh_s	annual precipitation of salt	0.10	m/yr
Δh_e	annual evaporation	1.22	m/yr
Δh_i	annual freshwater inflow	0.51	m/yr
ΔV_i	annual freshwater inflow	325	10^6 m^3/yr
Calculated Q_{LW} using equation (14)			
Brunt [1932]		74.3	W/m^2
Berliand and Berliand [1952]		73.1	W/m^2
Clark et al. [1974]		87.5	W/m^2
Efimova [1961]		67.7	W/m^2
Bunker [1976]		76.3	W/m^2
Anderson [1952]		74.8	W/m^2
Swinbank [1963]		72.1	W/m^2
Bignami et al. [1995]		108.0	W/m^2
USEPA [1984]		90.4	W/m^2

[a]The annual variations are marked with Δ. The numbers in parentheses indicate 1, average for the years 1996–2001, Israel Hydrological Service; 2, Dead Sea Works, PC; 3, Table 1; 4, *Hecht and Gertman* [2003], 5, *Konda et al.* [1994] and *Wilber et al.* [1999]; 6, *Steinhorn* [1981]; 7, *Payne* [1972] and *Ryan and Harleman* [1973].

evaporation rate derives from the uncertainty in the reflected short-wave radiation (albedo). Under typical conditions of predominantly light winds and relatively smooth sea surface, the average value used for albedo is 6%, i.e., α = 0.94 [*Payne*, 1972; *Rubin and Atkinson*, 2001; *Ryan and Harleman*, 1973]. A deviation of 1% from the latter value changes the rate of evaporation by 0.02 m/yr. A similar uncertainty in the calculated evaporation derives from a 0.05°C/yr uncertainty in the measured annual temperature rise of the water. The uncertainty related to the Bowen ration approach cannot be estimated due to the lack of direct measurements, but, according to *McNaughton and Laubach* [1998], "... using the Bowen ratio method to calculate surface energy fluxes will usually incur only minor errors."

[39] When incorporating the range of calculated Q_{LW} values from equation (14) into (23), and temperature rise of 0.25°C/yr, the calculated annual evaporation rate varies between 0.83–1.21 m/yr (Figure 7a). However, as discussed below, estimated surface inflow constrain the lower range of the calculated Δh_e to >1.1 m/yr. This range is close to the evaporation rates of 1.05 m/yr suggested by *Stanhill* [1994] based on heat balance calculations, and 1.23 m/yr estimated by *Yechieli et al.* [1998], but differs significantly from the rate of 2.0 m/yr based on pan evaporation by *Salameh and El-Naser* [1999].

4.3. Water Inflow

[40] Annual water inflow to the Dead Sea are calculated from the mass balance (4) using the salt annual precipitation (25) and rate of evaporation (23). It is useful to reduce (4) using (24) into the following form:

$$\Delta h_i = \Delta h_e + \frac{\rho_s - \rho}{\rho_w}\Delta h_s - \frac{\rho}{\rho_w}\left(\Delta h_l - \Delta h_p\right) + \frac{\Delta\rho}{\rho_w}h_t - \frac{\rho_r}{\rho_w}\Delta h_r \tag{26}$$

[41] Figure 7b presents the calculated total annual inflow for year 1999, as determined from the different formulations of Q_{LW} (equation (14) and Table 2) and the measured annual heating of 0.25°C/yr. The inflow range is 75–325 × 10^6 m^3/yr (note that $\Delta h_i = \Delta V_i/A$). Constraints on the minimum possible inflow derive from the minimum estimations of the observed surface inflow, which is 265 × 10^6 m^3/yr (Table 1). Thus the more realistic estimate of

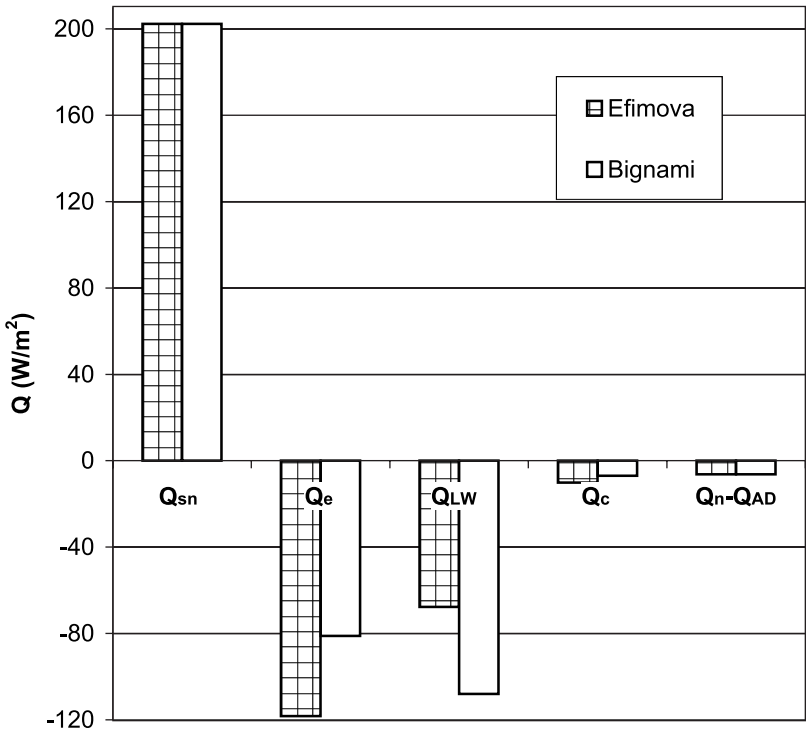

Figure 6. Energy flux components based on equations (12)–(14) and (20)–(22) and observed data. The highest and lowest estimates for long-wave radiation (from *Bignami et al.* [1995] and *Efimova* [1961], respectively) are presented along with the consequent variation in the evaporative and conductive heat fluxes.

inflow ranges from 265 × 10^6 m^3/yr, estimated from observations, to 323 × 10^6 m^3/yr, determined form the calculations. Since the inflow and evaporation are linked through equation (26), this also constrains the minimum evaporation rate to 1.10 m/yr (Figure 7a).

[42] Figure 8 plots the correlation between the hypothetical annual temperature change of the Dead Sea, $\Delta T/\Delta t$ (representing the net heat flux (10)), and the hypothetical annual inflow (representing the mass balance (26)). The different correlations (the inclined lines) derive from the various formulations for the net long-wave radiation. Also included in Figure 8 is the measured annual heating (0.25 ± 0.05°C/yr, the horizontal rectangle). The observed annual inflow range (265–475, Table 2) is plotted as vertical lines. The gray area represents the possible total inflow into the Dead Sea in 1999. The maximum calculated total inflow, 323 × 10^6 m^3/yr, is obtained when taking the lowest Q_{LW} value (the right inclined line) with an annual temperature rise of 0.25°C/yr. The uncertainty in the temperature rise (±0.05°C/yr) is translated to only ±8 × 10^6 m^3/yr. Higher subsurface inflow is not possible as it requires a higher evaporation rate, for which there is no source of energy flux.

4.4. Interannual Variations

[43] The calculations presented above for year 1999 were repeated for the other holomictic years 1996–2001 as well. As noted above, the constraint for the minimal total inflow derives from the minimum observed inflow (265 × 10^6 m^3/yr). The maximum calculated inflow for each year (Figure 9), is derived from the use of the formulation which yields the lowest long-wave radiation [*Efimova*, 1961] (see Table 2). The average interannual maximum inflow is 325 × 10^6 m^3/yr ±10%. This variability is due to the interannual variation in the measured meteorological and hydrographical parameters over and in the Dead Sea.

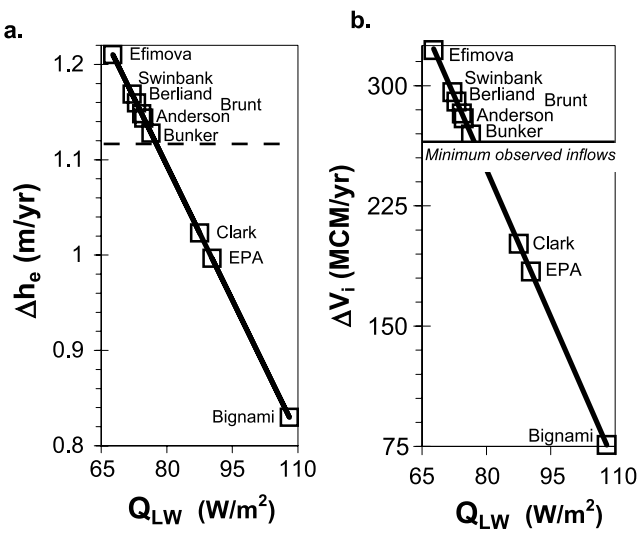

Figure 7. Variation in the calculated (a) rate of evaporation and (b) freshwater inflow with respect to the different net long-wave radiation. The different formulations of long-wave radiation (equation (14)) are indicated. Higher estimation of net long-wave radiation relates to less evaporation (equation (23)) and thus less inflow (equation (26)) and vice versa.

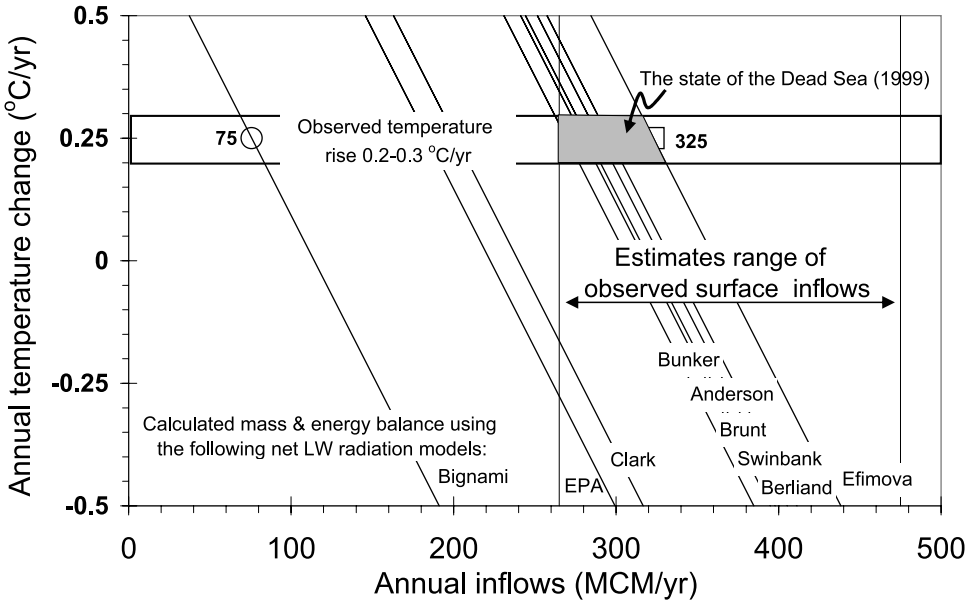

Figure 8. Correlation between hypothetical annual temperature change of the Dead Sea and annual inflow derived from different formulations for the net long-wave radiation for year 1999. The measured annual heating is depicted as the horizontal rectangular. The observed annual inflow range is plotted as vertical lines. The gray area represents the possible total inflow into the Dead Sea.

Accordingly, the average unobserved subsurface inflow for this period range from zero to a maximum of 60×10^6 m^3/yr.

4.5. Dead Sea at High Water Levels (pre-1950)

[44] During the beginning of the 20th century, the Dead Seawater level was relatively stable and the lake extended also into the shallow southern basin. Here we analyze the Dead Sea balances during this period, assuming steady state conditions [*Neumann*, 1958]. A rough estimation of the rate of evaporation is given from water balance considerations. As a terminal lake under steady state conditions, evaporation equals inflow ($\Delta m_i = \Delta m_e$), and the net heat flux is zero ($\Delta Q_n - \Delta Q_{AD} = 0$). The salt contribution entering with the enhanced freshwater inflow and the precipitating minerals were negligible ($\Delta m_s = 0$), and the industrial activity (Δm_p, Δm_r) was minimal. Applying the formulation described above ((4) and (23)) under the steady state conditions, it is possible to express the inflow (Δm_i) as a function of surface temperature and meteorological parameters:

$$\Delta m_i = \frac{\Delta t}{L_e} \frac{Q_{SN} - Q_{LW}}{1 + B} \tag{27}$$

[45] Historical data for the Dead Sea during 1942–1946 are summarized by *Neumann* [1958]. The surface elevation at that time was ~392 m below sea level and the lake area (including the southern basin) was ~950 km^2. At that time, the lake was still stratified with a relatively diluted epilimnion. The density of the surface water ranged between 1140–1190 kg/m^3. The annual averages include T_a = 23.6–25.4°C; e_a = 15.9–14.1 mbar and T_s = 24.7–25.3°C [*Neumann*, 1958]. On the basis of the chemical composition [*Neev and Emery*, 1967] for 1960, the water activity of the surface water was $\beta \sim 0.73$. In the beginning of the 20th century the salinity was even lower with estimated water activity of $\beta \sim 0.8$. The solar radiation in the Dead Sea rift valley was higher by more than 10% than the present radiation [*Stanhill and Cohen*, 2001]. Using the above ranges, the estimated inflow from energy balance calculations (27) falls in the range of 1550–1750 $\times$ 10^6 m^3/yr. Accordingly, despite the lower average surface temperature, the evaporation rate was 1.6–1.85 m/yr, which is higher than present-day evaporation (1.1–1.2 m/yr). The above derived values for the beginning of the 20th century compare well with previous estimates of inflow (1580 $\times$ 10^6 m^3/yr [*Neumann*, 1958]) and evaporation rates (1.57–1.98 m/yr [*Stanhill*, 1994]) for the same period.

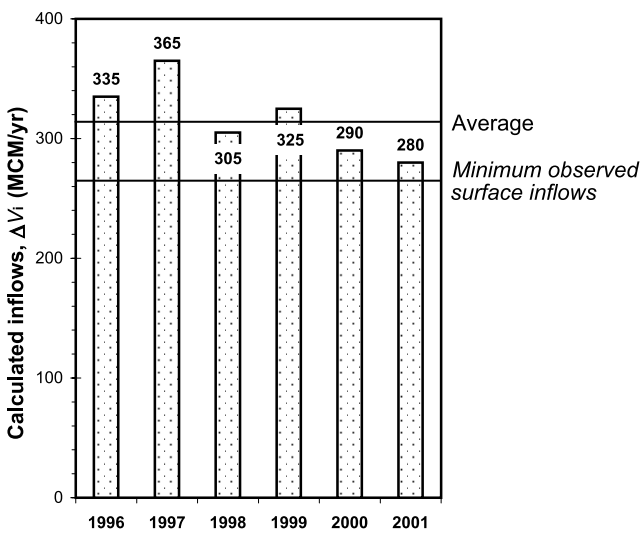

Figure 9. Maximum inflow (ΔV_i) calculated for the different holomictic years (1996–2001), based on the formulation of minimum net long-wave radiation [*Efimova*, 1961].

[46] The higher solar radiation during the early 20th century has a significant impact on the calculated evaporation rate. Keeping the measured parameters for that period, and using the reduced present-day solar radiation, reduces evaporation rate to 1.35–1.6 m/yr. This means that for the historical inflow and present solar radiation, the surface level of the Dead Sea would be higher and the area would be larger than those of the early 20th century. Thus the increased evaporation rate during the early 20th century should be attributed not only to the higher surface water activity, but also to the higher solar radiation reaching the Dead Sea surface at that period.

5. Summary and Conclusions

[47] The existing estimations of the water balance of the Dead Sea are widely variable and reflect the unknown subsurface water inflow and rate of evaporation. The situation is further complicated by the continuous salt precipitation from the Dead Sea hypersaline brine which raises the Sea bottom, and the industrial activity in the southern Dead Sea basin. The industries pump brine from the Dead Sea into evaporation ponds and discharge the concentrated brines back to the Dead Sea.

[48] We presented here a framework for the calculations of the total inflow and rates of evaporation and salt accumulation in a hypersaline lake with application to the Dead Sea, using energy and mass balance considerations. The application of the formulation to the Dead Sea is simplified since, on an annual basis, the relatively low inflow has very small effect on the salt and energy balances. The annual inflow are much lower than the total volume of the Dead Sea (<1%), while the temperature difference between the inflowing water and the bulk lake is usually <10°C. The mass of salt carried in by such low inflow is negligible compared to the high total salt content of the Dead Sea.

[49] The terms of the energy budget are calculated using meteorological and hydrographical data collected by a buoy located in the middle of the Dead Sea. The data set for the holomictic years 1996–2001 is recorded every 20 min and is the most detailed record of the Dead Sea. The heat of evaporation is calculated using Bowen's approach that eliminates the poorly constrained wind function from the heat balance. Since we do not have a direct measurement of the net long-wave radiation, we apply existing formulations that rely on meteorological data.

[50] The total annual inflow into the Dead Sea is 265–335 $\times$ 10^6 m^3/yr, corresponding to evaporation rates of 1.1–1.2 m/yr. The range of values derives mainly due to the variations between different formulations of the net long-wave radiation. A maximum subsurface inflow of 60 $\times$ 10^6 m^3/yr is deduced from the maximal total inflow and minimal estimate of observed surface inflow (265 $\times$ 10^6 m^3/yr). Higher subsurface inflow is impossible as it requires higher evaporation rate, for which there is no source of energy.

[51] Salt precipitation rate is 0.1 m/yr (per m^2). The accumulation of a salt layer at the bottom of the Dead Sea implies that the net rate of decrease in the lake's volume (height) is even higher than may be deduced from water level decline. Accordingly, the water deficit of the lake is nearly 690 $\times$ 10^6 m^3/yr. It should be noted that some 250 $\times$ 10^6 m^3/yr of this deficit are due to the activity of the chemical industries in the southern basin of the Dead Sea, equivalent to water level drop of ~0.4 m/yr. Thus, without the current industrial activity, lake level drop would be ~0.6 m/yr.

[52] Higher evaporation rate during the early 20th century, when the Dead Sea level was stable at a higher position, is attributed not only to the lower salinity, but also to the higher solar radiation reaching the Dead Sea surface at that period.

[53] To reduce the uncertainties in the mass and energy balances, we intend to add to our meteorological buoy the measurements of the net long-wave radiation over the Dead Sea.

Notation

A	surface area of the Dead Sea.
ΔA	annual change of the surface area.
B	Bowen ratio.
C	cloud cover.
c_b	Bowen's constant.
c_p	specific heat capacity of the brine.
e_a	atmospheric vapor pressure.
e_{sat}	saturation vapor pressure.
e_{brine}	saturation vapor pressure above the saline lake.
E_n	annual energy change.
$f(w)$	wind function.
Δh_l	water level drop.
Δh_s	annual precipitation of salt.
Δh_e	annual evaporation.
Δh_i	annual freshwater inflow.
Δh_s	salt precipitation raises the floor of the lake.
k_b	Boltzmann coefficient.
L_e	latent heat of vaporization.
m_t	total mass of the brine.
m_w	mass of fresh water.
m_s	mass of dissolved salt.
Δm_e	mass of water evaporated.
Δm_i	mass of water inflow.
Δm_p	mass of pumped Dead Sea brine.
Δm_r	mass of rejected end brines.
Δm_s	mass of dissolved salts.
Δm_t	change of the total mass.
P	atmospheric pressure.
Q_{AD}	advective heat flux.
Q_c	conductive heat flux.
Q_e	evaporative heat flux.
Q_{LW}	net long-wave radiation.
Q_n	net heat flux.
Q_S	measured short-wave radiation.
Q_{SN}	net short-wave radiation.
RH	relative humidity.
S	salinity of the brine.
S_i	salinity of the inflow.
S_n	new salinity of the brine.
S_r	salinity of rejected end brines.
ΔS	change in the salinity of the brine.
Δt	time period (year).
T_a	air temperature.
T_i	inflow water temperature.
T_r	reject end brine temperature
T_s	surface water temperature.
ΔT	change in surface water temperature.

V_t total volume of the brine.
ΔV_l volume loss as appears from the Dead Sea level drop.
ΔV_s volume of salt precipitated.
ΔV_p volume pumped.
ΔV_r volume of rejected end brines.
ΔV_i freshwater inflow.
α fraction of Q_s that penetrates into the water surface.
β water activity.
ε emissivity of water surface.
ρ bulk density of the brine.
$\Delta\rho$ changes in the density of brine.
ρ_w freshwater density.
ρ_s halite (solid) density.
ρ_r rejected end brines density.

[54] **Acknowledgments.** Scott Wells, Nathan Paldor, Ilan Setter, Yitzhak Mahrer, Elad Shilo, and Stuart Wollman are acknowledged for fruitful discussions. Alon Rimmer is greatly acknowledged for detailed review with suggestions that significantly improved the paper. Two anonymous reviewers are acknowledged for their reviews. Marc Parlange, Editor in Chief, is greatly acknowledged for handling of the manuscript. This study was partly supported by the U.S. Agency for International Development, the Middle East Regional Cooperation program (MERC project TA-MOU-03-M23-024) granted to American Near East Refugee Aid (ANERA) for the benefit of FoEME, and the Israel Science Foundation (grant 902/05).

References

Alpert, P., H. Shafir, and D. Issahary (1997), Recent changes in the climate at the Dead Sea—A Preliminary Study, *Clim. Change*, *37*, 513–537.

Anati, D. A. (1997), The hydrography of a hypersaline lake, in *The Dead Sea: The Lake and Its Setting*, edited by T. Niemi, Z. Ben-Avraham, and J. R. Gat, pp. 89–103, Oxford Univ. Press, New York.

Anati, D. A., and M. Stiller (1991), The post-1979 thermohaline structure of the Dead Sea and role of double-diffusive mixing, *Limnol. Oceanogr.*, *36*, 342–354.

Anderson, E. R. (1952), Energy budget studies, in *Water Loss Investigations: Lake Hafner Studies*, *U.S. Geol. Surv. Prof. Pap.*, *269*, 71–119.

Assouline, S. (1993), Estimation of lake hydrologic budget terms using the simultaneous solution of water, heat and salt balances and a Kalman filtering approach: Application to Lake Kinneret, *Water Resour. Res.*, *29*, 3041–3048.

Barenbrug, A. W. T. (1974), *Psychrometry and Psychrometric Charts*, 3rd ed., Cape and Transvaal, Cape Town, S. Afr.

Berliand, M. E., and T. G. Berliand (1952), Measurement of the effective radiation on the Earth with varying cloud amounts (in Russian), *Izv. Akad. Nauk. SSSR, Ser. Geofiz.*, *1*, 64–78.

Beyth, M. (1980), Recent evolution and present stage of Dead Sea brines, in *Hypersaline Brines and Evaporitic Environments*, edited by A. Nissenbaum, pp. 155–166, Elsevier, New York.

Beyth, M., I. Gavrieli, D. Anati, and O. Katz (1993), Effects of the December 1991–May 1992 floods on the Dead Sea vertical structure, *Isr. J. Earth Sci.*, *42*, 45–47.

Bignami, F., S. Marullo, R. Santoletri, and M. E. Schiano (1995), Longwave radiation budget in the Mediterranean Sea, *J. Geophys. Res.*, *100*, 2501–2514.

Bowen, I. S. (1926), The ratio of heat losses by conduction and by evaporation from any water surface, *Phys. Rev.*, *27*, 779–787.

Brunt, D. (1932), Notes on radiation in the atmosphere, *Q. J. R. Meteorol. Soc.*, *58*, 389–420.

Bunker, A. F. (1976), Computation on surface energy flux and annual air-sea cycle in the North Atlantic Ocean, *Mon. Weather Rev.*, *104*, 1122–1140.

Businger, J. A. (1973), Turbulent transfer in the atmospheric surface layer, in *Workshop on Micrometeorology*, edited by D. A. Haugen, pp. 67–100, Am. Meteorol. Soc., Boston, Mass.

Clark, N. E., L. Eber, R. M. Laurus, J. A. Renner, and J. F. T. Saur (1974), Heat exchange between ocean and atmosphere in the eastern North Pacific for 1961–71, *NOAA Tech. Rep. NMFS*, *SSRF-682*.

Dalin, Y. (1988), Valuation of expected floods into the Dead Sea (in Hebrew), *Rep. NCRD 10-82*, pp. 5–24, Negev Cent. for Reg. Dev., Beer Sheva, Israel.

Efimova, N. A. (1961), On methods of calculating monthly values of net longwave radiation (in Russian), *Meteorol. Gidrol.*, *10*, 28–33.

Gavrieli, I. (1997), Halite deposition in the Dead Sea, 1960–1993, in *The Dead Sea: The Lake and Its Setting*, edited by T. Niemi, Z. Ben-Avraham, and J. R. Gat, pp. 161–170, Oxford Univ. Press, New York.

Gavrieli, I., and A. Oren (2004), The Dead Sea as a dying lake, in *Dying and Dead Seas: Climatic Versus Anthropogenic Causes*, edited by J. C. J. Nihoul, P. O. Zavialov, and P. P. Micklin, pp. 287–305, Springer, New York.

Gavrieli, I., A. Bein, and A. Oren (2005), The deteriorating Dead Sea basin: Limnological and environmental changes and the expected impact of the "Peace Conduit," *Mitig. Adapt. Strategies Global Change*, *10*, 3–22.

Gertman, I., and A. Hecht (2002), The Dead Sea hydrography from 1992 to 2000, *J. Mar. Syst.*, *35*, 169–181.

Hecht, A., and I. Gertman (2003), Dead Sea meteorological climate, in *Fungal Life in the Dead Sea*, edited by E. Nevo, A. Oren, and S. P. Wasser, pp. 68–114, A.R.G. Gantner, Ruggell, Liechtenstein.

Holtzman, R., U. Shavit, M. Segal-Rozenhaimer, I. Gavrieli, E. Salameh, R. Daud, A. Marie, E. Farber, and A. Vengosh (2005), Mixing processes along the lower Jordan River, *J. Environ. Qual.*, *34*, 897–906.

Klein, M. (1998), Water balance of the upper Jordan River Basin, *Water Int.*, *23*, 244–248.

Konda, M., N. Imasato, K. Nishi, and T. Toda (1994), Measurements of the sea surface emissivity, *J. Oceanogr.*, *50*, 17–30.

Levy, Y. (1992), Modern sedimentation in the Dead Sea, 1982–1989, *Tech. Prog. Rep. TR-GSI/7/92*, Isr. Geol. Surv., Jerusalem.

McNaughton, K. G., and J. Laubach (1998), Unsteadiness as a cause of non-equality of eddy diffusivities for heat and vapor at the base of an advective inversion, *Boundary Layer Meteorol.*, *88*, 479–504.

Morton, F. I. (1983), Operational estimates of lake evaporation, *J. Hydrol.*, *66*, 77–100.

Neev, D., and K. O. Emery (1967), The Dead Sea depositional processes and environments of evaporites, *Bull. Geol. Surv.*, *41*.

Neumann, J. (1958), Tentative energy and water balances for the Dead Sea, *Bull. Res. Counc. Isr.*, *7G*, 137–163.

Payne, R. E. (1972), Albedo of the sea surface, *J. Atmos. Sci.*, *29*, 959–970.

Rubin, H., and J. Atkinson (2001), *Environmental Fluid Mechanics*, 728 pp., Marcel Dekker, New York.

Ryan, P. J., and D. R. F. Harleman (1973), An analytical experimental study of transient cooling pond behavior, *Rep. 161*, R. M. Parsons Lab., Dep. of Civ. Eng., Mass. Inst. of Technol., Cambridge.

Salameh, E., and H. El-Naser (1999), Does the actual drop in the Dead Sea level reflect the development of water sources within its drainage basin?, *Acta Hydrochim. Hydrobiol.*, *27*, 5–11.

Salameh, E., and P. Udluft (1985), A hydrodynamic pattern of the central part of Jordan, *Geol. Jahrb. Reihe C*, *38*, 39–53.

Salhotra, A. M., E. E. Adams, and D. R. F. Harleman (1985), Effect of salinity and ionic composition on evaporation: Analysis of the Dead Sea evaporation pans, *Water Resour. Res.*, *21*, 1336–1344.

Salhotra, A. M., E. E. Adams, and D. R. F. Harleman (1987), The alpha, beta, gamma of evaporation from saline water bodies, *Water Resour. Res.*, *23*, 1769–1774.

Stanhill, G. (1994), Changes in the rate of evaporation from the Dead Sea, *Int. J. Climatol.*, *14*, 465–471.

Stanhill, G., and S. Cohen (2001), Global dimming: A review of the evidence for a widespread and significant reduction in global radiation with discussion of its probable causes and possible agricultural consequences, *Agric. For. Meteorol.*, *107*, 255–278.

Steinhorn, I. (1981), A hydrographical and physical study of the Dead Sea during destruction of its long-term meromictic stratification, Ph.D. thesis, Weizmann Inst. of Sci., Rehovot, Isr.

Steinhorn, I. (1983), In situ salt precipitation at the Dead Sea, *Limnol. Oceanogr.*, *28*, 580–583.

Steinhorn, I. (1991), On the concept of evaporation from fresh and saline bodies, *Water Resour. Res.*, *27*, 645–648.

Steinhorn, I., and J. R. Gat (1983), The Dead Sea, *Sci. Am.*, *249*, 102–109.

Steinhorn, I., et al. (1979), The Dead Sea: Deepening of the mixolimnion signifies the overture to overturn of the water column, *Science*, *206*, 55–57.

Stiller, M., and Y. C. Chung (1984), Radium in the Dead Sea: A possible tracer for the duration of meromixis, *Limnol. Oceanogr.*, *29*, 574–586.

Stiller, M., J. R. Gat, and P. Kaushansky (1997), Halite precipitation and sediment deposition as measured in sediment traps deployed in the Dead Sea: 1981–1983, in *The Dead Sea–The Lake and Its Setting*, edited by T. Niemi, Z. Ben-Avraham, and J. R. Gat, pp. 171–183, Oxford Univ. Press, New York.

Stumm, W., and J. J. Morgan (1981), *Aquatic Chemistry*, John Wiley, New York.

Swinbank, W. C. (1963), Longwave radiation from clear sky, *Q. J. R. Meteorol. Soc.*, *89*, 339–348.

U.S. Environmental Protection Agency (USEPA) (1984), Proceedings of Stormwater and Water Quality Model Users Group Meeting April 12–13, 1984, *Rep. EPA-600/9-85-003*, Washington, D. C.

Wilber, A. C., D. P. Kratz, and S. K. Gupta (1999), Surface emissivity maps for use in satellite retrievals of longwave radiation, *NASA Tech. Rep.*, *NASA/TP-1999-209362*.

Winter, T. C., D. C. Buso, D. O. Rosenberry, G. E. Likens, A. M. J. Sturrock, and D. P. Mau (2003), Evaporation determined by the energy-budget method for Mirror Lake, New Hampshire, *Limnol. Oceanogr.*, *48*, 995–1009.

Yechieli, Y., I. Gavrieli, B. Berkowitz, and D. Ronen (1998), Will the Dead Sea die?, *Geology*, *26*, 755–758.

Y. Dvorkin, I. Gavrieli, N. G. Lensky, and V. Lyakhovsky, Geological Survey of Israel, Malkhei Yisrael Street 30, Jerusalem 95501, Israel. (nadavl@gsi.gov.il)

I. Gertman, Israel Oceanographic and Limnological Research, Haifa 31080, Israel.